

Unified Longitudinal Flight-dynamic and Aeroelastic Analysis of a PrandtlPlane Configuration

Rocco Bombardieri
University Carlos III of Madrid
PhD student
Av. de la Universidad 30, 28911 Leganés, MA

Francesco Auricchio
University Federico II of Naples
Visiting graduate student

Rauno Cavallaro
University Carlos III of Madrid
Assistant Professor
rauno.cavallaro@uc3m.es

ABSTRACT

Longitudinal flight-dynamic behavior of a *flexible* joined-wing PrandtlPlane configuration is here investigated. The baseline model was previously designed by partner universities through several optimizations and ad-hoc studies in the field of aeroelasticity and flight mechanics.

First, longitudinal stability analyses are performed on the rigid configuration. The possibility to rely on a frequency-domain panel method for the evaluation of aerodynamic forces requires particular care in the rational function approximation method used to interpolate forces at low reduced frequencies. Moreover, short-period poles are stable for the considered speed range but differences in their characteristics have been found, compared to solvers relying on steady panel methods, which was considered as due to the contribution of unsteady aerodynamic derivatives that are only present in the first approach.

As a second step, unified analysis considering the flexibility of the vehicle are carried out. Given the presence of the short-period mode, flutter speed increases if compared to the cantilever wing system. Reciprocally, the short-period mode is influenced by the vehicle's flexibility and its frequency and damping ratio change above the considered speed interval. Values of the damping ratio, however, always fulfill the flying quality level requirements.

Another load condition of the same configuration is studied, characterized by different inertial properties and margin of stability. Short period is stable and similar to what seen for the previous configuration. Unified analyses highlight flutter of the third elastic mode in the considered speed range. Cause is associated to the different modal properties of the layout caused by different load distribution on the two wings. Again, elasticity is found to influence the short-period response but values of the damping comply with flying quality requirements.

KEYWORDS: *PrandtlPlane, Box Wing, Flutter, Rational Function Approximation, Flexible Flight-dynamics.*

NOMENCLATURE

$[A(\bar{s})]$ - Generalized Aerodynamic Force (GAF) matrix in the Laplace domain

$[A_0]$ - Aerodynamic stiffness matrix

$[A_1]$ - Aerodynamic damping matrix

$[A_2]$ - Aerodynamic mass matrix

\bar{c} - Reference length

\tilde{f} - Generalized aerodynamic force vector in the Laplace domain

k - Reduced frequency

M_c - Mach Cruise

M_d - Mach Diving

q_∞ - asymptotic dynamic pressure

r - point position vector in the body reference system

s - Laplacian variable

$[T_i^L]$ - GAF rotation matrix from aerodynamic mesh reference system to the main axes reference system

V_∞ - asymptotic speed
 x_R^L - Rigid modal coordinates vector
 β_i - Lag coefficient in Roger's RFA

η - Modal coordinate vector
 η_E - Elastic modal coordinate vector
 ω_{SP} - Short-period frequency

INTRODUCTION

Flight-dynamics and aeroelasticity play an important role in aircraft design; historically, they have been studied, developed and used separately in the design process. Nevertheless, the interest in developing a unified model, able of studying the flight-dynamics of a flexible body, is not recent. In [21-22], Milne presented one of the first contributions on the topic and introduced one of the most complex aspects of flexible aircraft dynamics: the choice of the reference frame. Etkin [23] implemented the *mean axes frame*, as proposed by Milne, and decided to describe deformations by a superposition of structure's normal modes. Waszak and Schmidt also presented in 1988 an alternative approach [24]: the model was obtained through Lagrange's equations and they used a strip theory to express aerodynamic terms. In 1966 Meirovitch and Nelson published an alternative approach, [25]: a hybrid (ordinary and partial) set of differential equations was used to analyse the coupling of rigid-body rotations and elastic deformations for a spacecraft with flexible appendages, which was extended to a generic flexible body in [26].

One of the main arguments to uncouple flight dynamics and aeroelasticity has always been the typical different frequency scale of structural elastic modes and rigid behaviour of an aircraft. Anyway, as low structural weight is pushed more and more to the limits in modern designs, the necessity of a unifying design tools becomes more and more pressing, as aircraft tend to get more flexible and the effects of rigid-body and elastic mode coupling becomes more relevant.

This coupling seems to be inherently relevant also on some new aircraft layouts, as Joined Wings [27] in general, and in this specific case, PrandtlPlanes¹.

Relatively to the PrandtlPlane configuration, both aeroelastic and flight-dynamic properties have been separately studied in several efforts. On the aeroelastic perspective, [6] was one of the first attempt to study flutter on a "realistic" configuration, followed by [12], in which a parametric study was performed to efficiently increase flutter speed. On the flight-dynamic side, [11] designed the mobile surfaces complying with a set of handling qualities and requirements at various flight conditions.

Paper [14] was a first attempt to convey towards a unified aeroelastic flight-dynamic perspective: considerations on flutter properties on a free-flying configuration were made in longitudinal flight; [15] extended the study to the antisymmetric condition. Both efforts were, however, mostly devoted to aeroelastic considerations, as they were not completely considering all the contributions given by the equations of rigid-body motion, characteristics of a flight-dynamic approach.

1.1 Contributions of the present study

Considering the literature on design of *PrandtlPlane* [29,30] a significant amount of work has been carried out in the past years, thus a realistic reference configuration is available for both aeroelastic and flight-dynamic analyses.

This study features a PrandtlPlane layout similar to the one studied in [9-12] as it represents an ideal starting point for a first approach to flight dynamics of the flexible configuration. An in-house state-space tool is designed from scratch, able to solve the equations of motion of a flexible aerodynamic body and evaluate its stability properties. Such tool relies on a Doublet Lattice Method (DLM) for the evaluation of unsteady aerodynamic forces in the frequency domain.

The contributions of this paper are here outlined.

- Rigid longitudinal flight-dynamic analyses are performed on the PrandtlPlane configuration relative to its Maximum Take-off Weight (MTOW) with maximum payload condition. Stability results are validated and compared to literature. Considerations are made on the necessity of a good interpolation of the unsteady aerodynamic forces over the considered range of reduced frequencies in order to achieve good results.

¹ The interest of the scientific community for the potential of this configuration is current as demonstrated by the ongoing project **Parsifal** (Prandtlplane ARchitecture for the Sustainable Improvement of Future AirLanes) financed by EU within the Horizon 2020 framework.



- Unified longitudinal flight-dynamic analyses on the *flexible* configuration are performed. Influence of the elasticity of the vehicle on the flight-dynamic properties is discussed; considerations are made on the vehicle's flight qualities.
- Studies on flight-dynamics and aeroelasticity interaction are extended also to the Quasi-zero Fuel Weight (QZFW) condition, in which a reduced amount of fuel is carried by the aircraft.

2 THEORETICAL HIGHLIGHTS REGARDING THE PRESENT COMPUTATIONAL TOOLS

In this section, the computational tools used in the paper are presented. An in-house unified state-space tool solves the equations of motion of a flexible aerodynamic body with a given number of degrees of freedom (*ndof*). The framework will be addressed as Unified Flexible Flight Dynamics (UFFD). In-house written DLM tool is used for the evaluation of unsteady aerodynamic forces at given reduced frequencies [1-2]. To interpolate these forces over the range of considered frequencies different Rational Function Approximation (RFA) methods are implemented, mainly based on Roger's approach [3]. As a mean for comparison of the rigid flight-dynamic properties only, a state-space representation of the classical equations of motion of a vehicle is also implemented; in such tool, the aerodynamic forces are provided in form of aerodynamic derivatives and calculated by AVL, an open source vortex-lattice method (VLM) capable to perform trim calculations analyses [17]. This tool will be addressed as Rigid Flight Dynamics (RFD).

A theoretical description of the tools is given in the following; however, for a more-in-depth full formulation of UFFD, the reader is referred to [20].

2.1 Unified Flexible Flight-Dynamics Tool

A unified model for flight dynamics, considering the flexibility of the aircraft, can be derived through several different approaches such as integrating the flexibility of the vehicle in a classical flight-dynamic model [28] or, alternatively, properly considering the rigid-body modes in an aeroelastic problem. Each approach, however, presents some criticalities as theoretical inconsistencies due to some fundamental differences and overlaps between the two disciplines exist. In this study, the model is derived from scratch. *Lagrangian equations* of mechanics are the starting point to define such model, as they naturally allow to choose both rigid-body and elastic variables as the generalized coordinates of the problem.

Although the choice of the frame describing the flight dynamics of the vehicle is arbitrary, the equations governing the dynamics of the flexible aircraft can be simplified with an ad-hoc choice of the vehicle-fixed frame. In references [21-22] it is noted that for an elastic body always exists a coordinate frame such that the relative linear and angular momenta, due to elastic deformation, are zero at every instant. This non-inertial reference system is called *mean axes* frame and its origin coincides with the instantaneous centre of mass of the vehicle. These axes move in phase with the body motion but they are not attached to any fixed point in the aircraft. These properties, formalized in Eq. 1, can sensibly simplify the equations of motions for the elastic vehicle.

$$\begin{cases} \int_{Vol} \frac{d\mathbf{r}}{dt} \Big|_B \rho_V dV = \mathbf{0} \\ \int_{Vol} \mathbf{r} \times \frac{d\mathbf{r}}{dt} \Big|_B \rho_V dV = \mathbf{0} \end{cases} \quad (1)$$

The main advantage of using the mean axes frame is the possibility to decouple the equations of motion governing the *rigid-body* degrees of freedom from the ones governing the *elastic* degrees of freedoms. The only coupling terms will be the *aerodynamic forces*, whose integration into the system of equations deserves some remarks.

2.2 Aerodynamic forces evaluation

Given a set of reduced frequencies k and one of structural modes n the DLM evaluates in the frequency domain the generalized aerodynamic force (GAF) matrix $Q_{nn}(ik)$, expressing the generalized aerodynamic force normalized by dynamic pressure at reduced frequency k . Anyway, to properly set up a linear state-space formulation of the unified model, a continuous dependence on k is required: this is pursued through a rational function approximation (RFA) method. In general, an RFA method provides the aerodynamic force matrix $[A(\bar{s})]$ such that $\tilde{\mathbf{f}}$, a vector in Laplacian domain

whose components are generalized aerodynamic forces associated with given n modal coordinates of the problem, is expressed as in Eq. 2.

$$\tilde{\mathbf{f}} = q_\infty [A(\bar{s})] \{\boldsymbol{\eta}\} \quad (2)$$

Where \bar{s} is the adimensional Laplace variable (which is complex), $\{\boldsymbol{\eta}\}$ is the vector containing the modal coordinates of the problem (both rigid and elastic) and q_∞ is the dynamic pressure. The representation of $[A(\bar{s})]$ given by the RFA is continuous, at least of the second order², function in the Laplace domain of as in Eq. 3.

$$[A(s)] = [A_0] + \frac{s\bar{c}}{2V_\infty} [A_1] + \left(\frac{s\bar{c}}{2V_\infty}\right)^2 [A_2] + H. O. T. \quad (3)$$

where $[A_0]$, $[A_1]$, $[A_2]$ are respectively the aerodynamic stiffness matrix, the aerodynamic damping matrix and the aerodynamic mass matrix. Without the higher order terms, Eq. 3 represents a *quasi-steady* formulation of the aerodynamic forces; conversely, the unsteady effects of the flow are caught by the higher order terms (or, commonly defined, lag terms) that can be differently obtained according to the adopted RFA method.

2.1 Rational Function approximation methods

The RFA methods used in this effort are based on the Roger approximation method. According to Roger's method the GAF matrix is represented in the frequency domain as in Eq. 4.

$$[A(s)] = [A_0] + \frac{s\bar{c}}{2V_\infty} [A_1] + \left(\frac{s\bar{c}}{2V_\infty}\right)^2 [A_2] + \sum_{i=1}^{Nlag} \frac{s}{s + \frac{\beta_i \bar{c}}{V_\infty}} [A_{2+i}] \quad (4)$$

where β_i are Lag coefficients chosen by the user. Given the values of $[A(ik)]$ by the DLM, for the selected set of reduced frequencies, a Least-Square (LS) method returns the *real* matrices $[A_i]$ whose polynomial interpolation as in Eq. 4 minimizes the "error" over the known GAF values.

An additional method is here implemented, called *Roger Mod*, which adds to the original set of LS constraint equations, over the values of $[A(ik)]$, a further constraint for the *derivative* of the interpolated GAF matrix. Such target derivative value is determined at $k = 0$ on the basis of a finite difference scheme of the given $[A(ik)]$. This method is defined to increase accuracy around the $k \rightarrow 0$ region, where most of the flight-mechanic physic is thought to be held.

2.2 State-space formulation for longitudinal dynamics and straight-and-level flight

The complete state-space formulation is reported in Eq. 5 for the case of longitudinal dynamics, straight-and-level flight and quasi-steady formulation of the aerodynamic forces. The relation implementing the lag terms of the aerodynamic forces is not given for the sake of clarity.

$$\begin{bmatrix} \left([M_{RR}^L] - q_\infty \left(\frac{\bar{c}}{V_\infty}\right)^2 \begin{bmatrix} [A_{2RR}][T_5^L] & [A_{2RR}][T_4^L] \\ [0]_{n_R} & [0]_{n_R} \end{bmatrix} \right) & \begin{bmatrix} q_\infty \left(\frac{\bar{c}}{V_\infty}\right)^2 [A_{2RE}] \\ 0_{n_R \times n_E} \end{bmatrix} & [0]_{2n_R \times n_E} \\ -q_\infty \left(\frac{\bar{c}}{V_\infty}\right)^2 [A_{2RR}][T_5^L] & [T_4^L] & \left([\bar{M}_S] - q_\infty \left(\frac{\bar{c}}{V_\infty}\right)^2 [A_{2RR}] \right) & 0_{n_E} \\ [0]_{n_E \times 2n_R} & 0_{n_E} & 0_{n_E} & I_{n_E} \end{bmatrix} \begin{Bmatrix} \dot{x}_R^L \\ \dot{\eta}_E \\ \dot{\eta}_E \end{Bmatrix} = \begin{bmatrix} [K_{RR}^L] + q_\infty \left[\frac{\bar{c}}{V_\infty} [A_{1RR}][T_3^L] \quad \frac{\bar{c}}{V_\infty} [A_{1RR}][T_2^L] + [A_{0RR}][T_1^L]\right] & \begin{bmatrix} q_\infty \frac{\bar{c}}{V_\infty} [A_{1RE}] \\ 0_{n_R \times n_E} \end{bmatrix} & \begin{bmatrix} q_\infty [A_{0RE}] \\ 0_{n_R \times n_E} \end{bmatrix} \\ q_\infty \left[\frac{\bar{c}}{V_\infty} [A_{1ER}][T_3^L] \quad \frac{\bar{c}}{V_\infty} [A_{1ER}][T_2^L] + [A_{0ER}][T_1^L]\right] & - \left([\bar{C}_S] - q_\infty \frac{\bar{c}}{V_\infty} [A_{1EE}] \right) & \left([\bar{K}_S] - q_\infty [A_{0EE}] \right) \\ [0]_{n_E \times n_R} & I_{n_E} & 0_{n_E} \end{bmatrix} \begin{Bmatrix} x_R^L \\ \dot{\eta}_E \\ \eta_E \end{Bmatrix} \quad (5)$$

In Eq. 5:

- x_R^L is the vector of the rigid modal coordinates;
- η_E is the vector of the elastic modal coordinates;

² Here the authors refer to the most popular RFA methods (Roger [3], Karpel [4,5]) which give a polynomial representation of the $[A(\bar{s})]$.

- $[M_{RR}^L]$ and $[K_{RR}^L]$ are the matrices representing the left-hand side of the linearized longitudinal flight dynamics equations of a rigid vehicle for straight-and-level flight [31];
- $[\bar{M}_s]$, $[\bar{D}_s]$, $[\bar{K}_s]$ are, respectively, the *modal* mass, damping and stiffness matrices of an elastic body;
- $[A_{iRR}]_{i=1,2,3}$ are the RFA interpolating matrices given in Eq. 3. *RR* stands for *rigid on rigid*, *RE* for *rigid on elastic* and so on.
- $[T_1^L]$, $[T_2^L]$, $[T_3^L]$, $[T_4^L]$, $[T_5^L]$ are the rotation matrices which perform the transformation of the generalized aerodynamic force matrix from the aerodynamic mesh coordinate system (where the DLM is performed) to the main axes.

3 DESCRIPTION OF THE ANALYZED PRANDTLPLANE CONFIGURATION

Object of the analysis is a typical PrandtlPlane configuration, whose artistic view is given in Fig. 1. It is a 250 passenger mid-long range (6000 nm) design with a MTOW of 230 tons, and it will be referred to as *PrP250*.



Figure 1: Artistic view of the PrP250 taken from [6]

The external surface and general layout were designed also with an MDO approach, as shown in [7-8]. Later the structure was fine-tuned [6,9] taking into account different constraints such as maximum stress, local buckling of stiffened panels, aileron efficiency, static aeroelasticity and flutter. Further work on the configuration flight mechanics was conducted in [10], while the mobile surfaces have been seized in [11] in order to comply with a given set of handling qualities at various flight conditions.

For the wing system, the original model from [6] is adopted. The wing box is described by beam elements and the inertial effects of fuel and non-structural systems are modelled through a combination of rigid elements and lumped masses, as illustrated in Fig. 2. The aerodynamic mesh is proved to have reached convergence of results. Such a model was originally used to perform linear flutter analysis on the configuration [12].

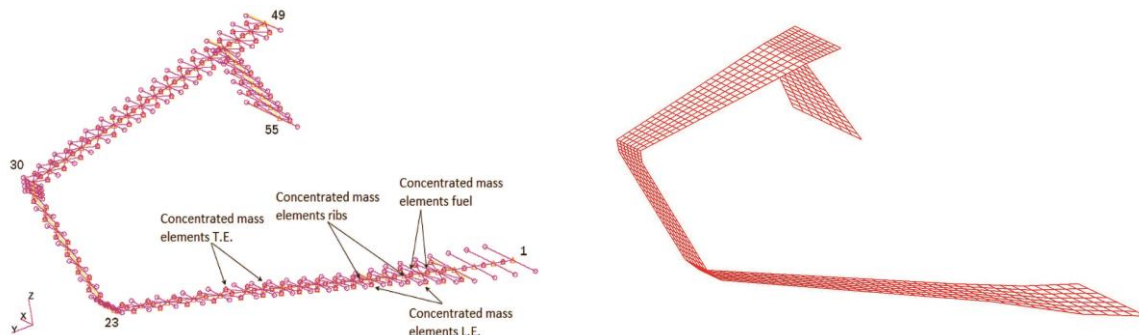


Figure 2: Structural model and aerodynamic mesh used for flutter analysis [12].

In order to take into account the rigid-body modes of the full aircraft, fuselage effects need to be retained. Since designing a structural model of a "realistic" fuselage for such aircraft configuration needs a series of specific investigations [13], as first approximation, it has been preliminary considered rigid, as done also in [14,15]. Fuselage overall weight (comprehensive of payload), inertial properties and position in respect to the wing system's centre of gravity have been extrapolated with arguments basing on similarity from [10,11], and ensuring a margin of static stability consistent with what found in literature for the given configuration [16]. Anyway, inertial properties of an aircraft may change to a large extent during the mission or from mission to mission. An adequate study should take into account the several possible load conditions of the aircraft, according to its flexibility diagram. In this contribution, two configurations are studied and compared. The Maximum Take-Off Weight (MTOW) with maximum payload configuration will be considered as the baseline. A second configuration is obtained unloading the wing system of the fuel. Only a residual amount of fuel is retained in the areas of the wing corresponding to the fuselage. This configuration will be addressed from now on, as the Quasi Zero Fuel Weight (QZFW) configuration. The two configuration's inertial properties are briefly reported in Table 1, where the indicated margin of stability is calculated using the mean aerodynamic chord of the wing system.

Table 1: PrP250 load cases

Configuration	Mass [tons]	Iyy (pitching) [kg*m ²]	Margin of stability
MTOW	230	35292980	15%
QZFW	151	20550520	5%

To model the above inertial properties, lumped mass elements have been appropriately placed in correspondence of both the fuselage and the model CoG. These points were, then, rigidly connected to the front wing and fin, ensuring, so, the desired rigid-body motions of the aircraft. A scheme of the conceptual layout is presented in Fig. 3.

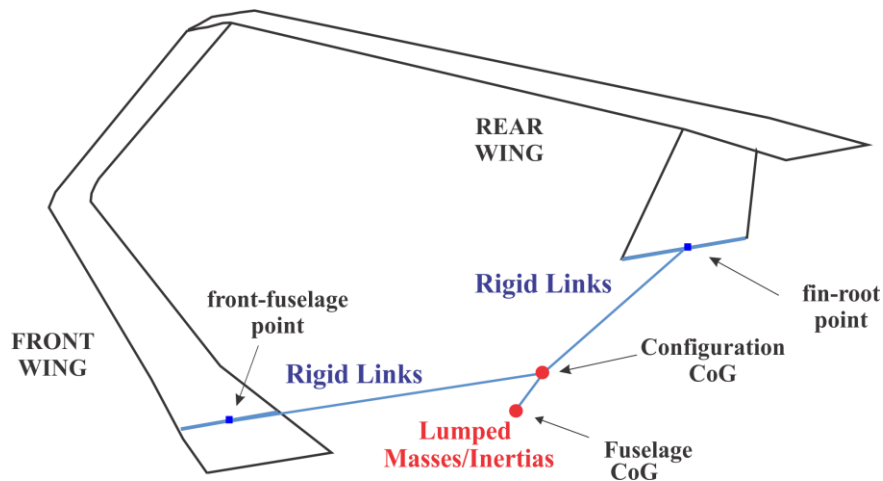


Figure 3: Conceptual model of the "free-flying" configuration.

Few words deserved to be spent in comparing the two configurations in exam under a modal point of view. In Fig. 4 it is shown how, not only the first four elastic modes present different relative frequencies, but, also the shape associated to these modes slightly changes. This is due to the fact that, both the mass of the configuration and the inertial distribution along the wing system have changed. Given the peculiar wing shape, the fuel is distributed differently along the two wings. Unloading them from its relative weight inherently changes their relative stiffness-to-weight ratio with effects on the system modal properties. This is particularly evident considering the shapes of modes III and IV. Given that, also the flutter behaviour of the two configurations is expected to be different

(effects of the fuel load distribution along the wing on the flutter behaviour of the PrandtlPlane wing system was already preliminary noticed in [12]).

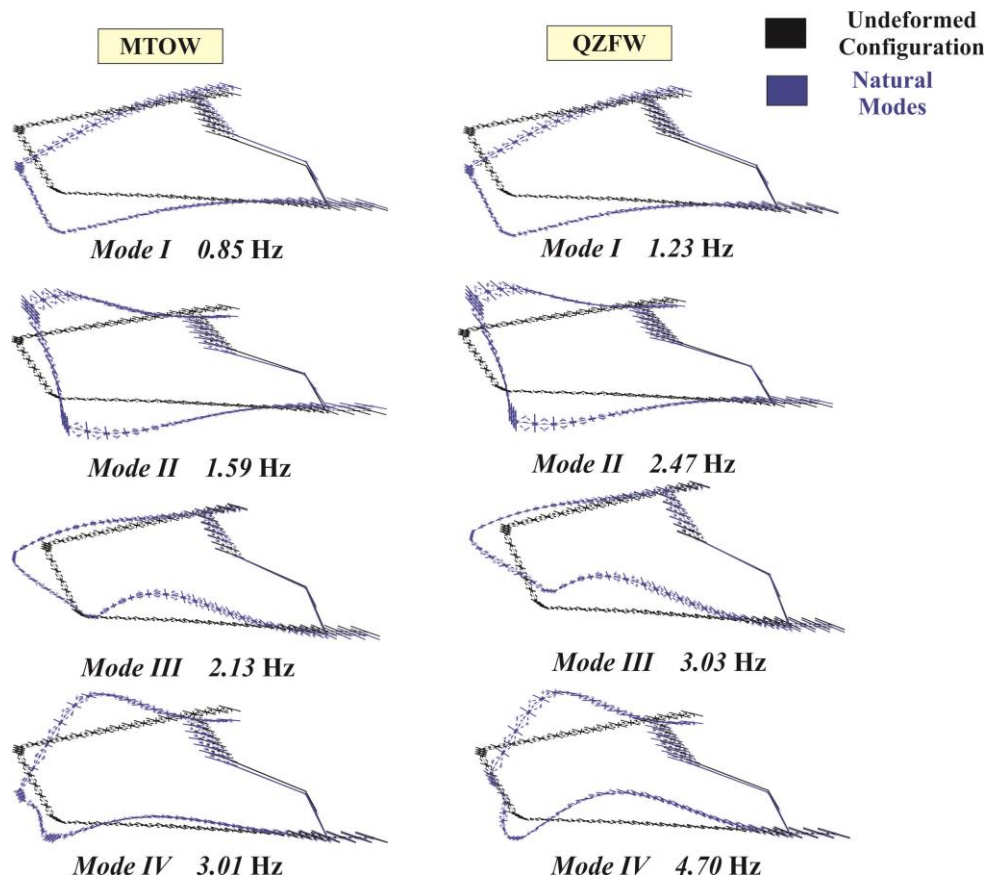


Figure 4: First five natural symmetric modes and associated frequencies for the Maximum Take Off Weight (MTOW) and Quasi Zero Fuel Weight (QZFW) configurations.

4 MTOW CONFIGURATION: LONGITUDINAL RIGID FLIGHT-DYNAMICS

The rigid flight-dynamics of the MTOW configuration is studied in this section; both a classical RFD model (VLM-AVL based aerodynamic model) and UFFD for rigid-body (DLM based aerodynamic model) have been employed. The aerodynamic mesh used in the VLM for RFD analysis is shown in Fig. 5 and the associated aerodynamic coefficients are listed in Table 2. As it can be noticed, the VLM only provides steady aerodynamic derivatives and contributions like $C_{M_{\dot{\alpha}}}$, $C_{L_{\dot{\alpha}}}$ are not, so, considered for RFD analyses.

UFFD is set using only the symmetric rigid-body modes of the configuration (3 DOFs), and thus the traditional rigid flight-dynamic equations are fully recovered. Different RFA methods are employed within the framework for result comparison.

When the DLM and VLM aerodynamic models are used for the evaluation of the aerodynamic forces, drag related terms can't be evaluated (for the intrinsic nature of panel methods' formulation). Main consequence is that aerodynamic coefficients relative to the considered reference condition ($C_{L_{ref}}$ and $C_{D_{ref}}$) are not considered and, thus, phugoid mode behaviour cannot be described.

The analyses are performed at sea level ($h = 0$ m) and cruise altitude ($h = 10500$ m); the velocity range covers part of the flight envelope [6]. The classical diving speed (V_D) is considered as the upper limit for this interval. At cruise altitude, the limit is imposed by the Mach number; cruise Mach number is $M_c = 0.85$ and $M_D = M_c + 0.05 = 0.9$. The associated True Air Speed is $V_D = 267.55$ m/s. At sea level, the limitation is directly imposed on speed, and gives $V_D = 1.25V_c = 245.1$ m/s. The following analysis aims to compare the rigid flight-dynamic properties provided by the two tools and

simultaneously to highlight potential effects of the different RFA methods.

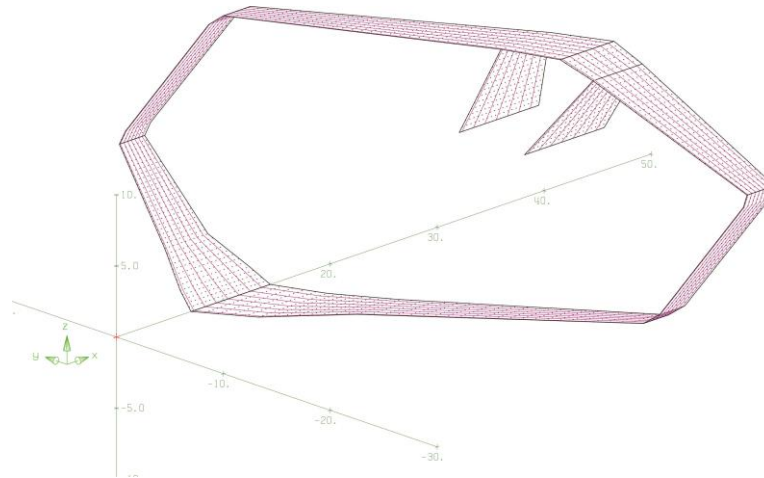


Figure 5: PrP250: AVL aerodynamic mesh.

Table 2: PrP250 MTOW: AVL rigid-body longitudinal stability derivatives

$C_{L\alpha}$	4.48 1/rad
$C_{M\alpha}$	-0.38 1/rad
C_{Lq}	5.94
C_{Mq}	-29.08

Given the values of the aerodynamic derivatives proposed in Table 2, some preliminary remarks about the flight-dynamic properties of this configuration follow. It is, indeed, possible to notice particularly large values of C_{Mq} and small values of $C_{M\alpha}$ if compared to traditional wing configurations. An investigation on flight qualities for rigid vehicle on a different class of PrandtlPlane configuration (*Light Sport Aircraft*) has been carried out in [16]: it was initially noted that, compared to aircraft of the same category, the PrandtlPlane wing system had an aerodynamic pitch-damping coefficient C_{Mq} about three time higher than the ones characteristic of a classical wing-tail layout because of the peculiar disposition of the lifting surfaces around its centre of gravity. High values of C_{Mq} influence the short-period response of the system. Considering the frequency in particular, it is well known that for flying quality reasons its value must be limited. For the longitudinal short-period approximation, the expression of the relative frequency is given in Eq. 6. It is evident that, for high values of C_{Mq} , one of the options to limit the value of the frequency is to directly operate on $C_{M\alpha}$ (given the fact that both the derivatives are negative in sign), reducing the static margin of stability of the configuration. This highlights the fact that PrandtlPlane configurations usually have smaller margins of stability than traditional simple wing-tail ones (Table 2). To the reduction of the margin of stability corresponds, given elementary flight-mechanics considerations, also a reduction of the values of C_{Lq} .

$$\omega_{SP} = \sqrt{-M_{\alpha} + Z_w M_q}; \quad (6)$$

First set of analysis is performed at sea level. The comparison between RFD and UFFD root loci is presented in Fig. 6: UFFD is executed with different RFAs, performed on the same set of reduced frequencies. This set was inherited from the 21-element set of values representative of the number of elastic modes that proved to give convergence of results in flutter analyses, for the given structural model.

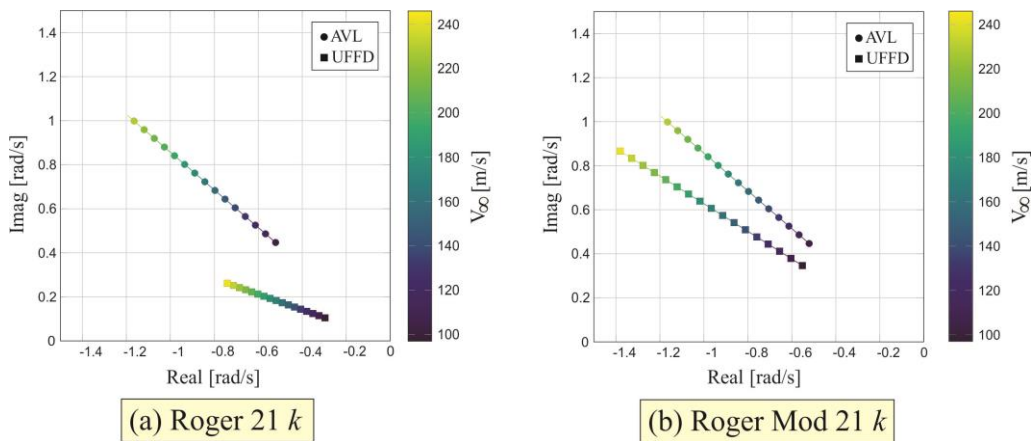


Figure 6: PrP250 MTOW, rigid flight-dynamics: comparison between RFD (AVL based aerodynamic model) and UFFD for rigid-body (DLM based aerodynamic model). 21 values of k , sea level.

In order to better understand the given results, also the different RFA interpolating functions for the elements $A_{2,3}$ and $A_{3,3}$ of the GAF matrix, as introduced in Eq. 3, are presented in Fig. 7 and Fig. 8. The tabulated values in the figures represent the specific GAF values at each considered reduced frequency k as calculated by the DLM, while the curves represent the different interpolating RFA functions adopted. The area of small reduced frequencies ($k \rightarrow 0$) is magnified. The importance of these coefficients in the characterization of the short period is justified by a quasi-steady interpretation of the RFA interpolation of the aerodynamic forces, as explained in [18]. These elements are related to classical aerodynamic derivatives; in particular $A_{2,3}$ at $k = 0$ is proportional to $C_{L\alpha}$ and its derivative to $C_{L\dot{\alpha}}$ and C_{Lq} ; $A_{3,3}$ at $k = 0$ is proportional to $C_{M\alpha}$ and its derivative to $C_{M\dot{\alpha}}$ and C_{Mq} .

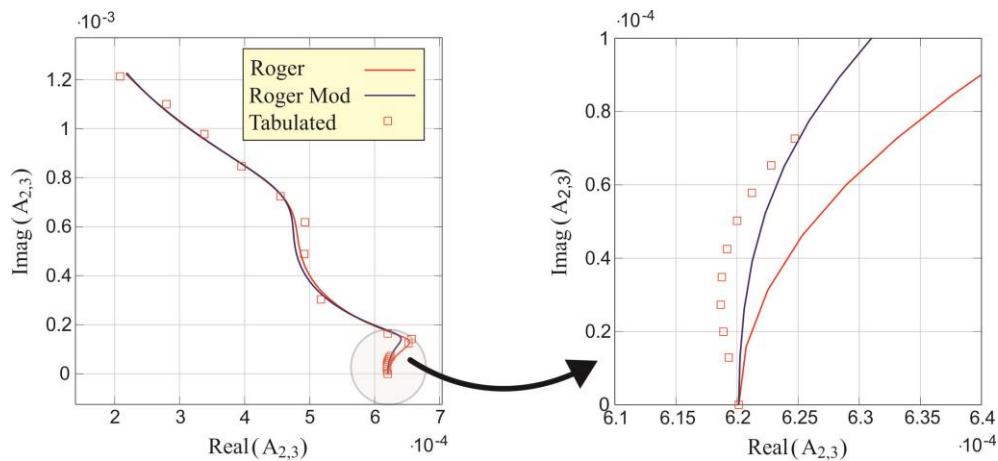


Figure 7: Comparison of different RFA methods on a set of 21 values of reduced frequencies and on the element $A_{2,3}$ (proportional to $C_{L\alpha}$). Magnification of the area relative to small reduced frequencies is provided ($k \rightarrow 0$).

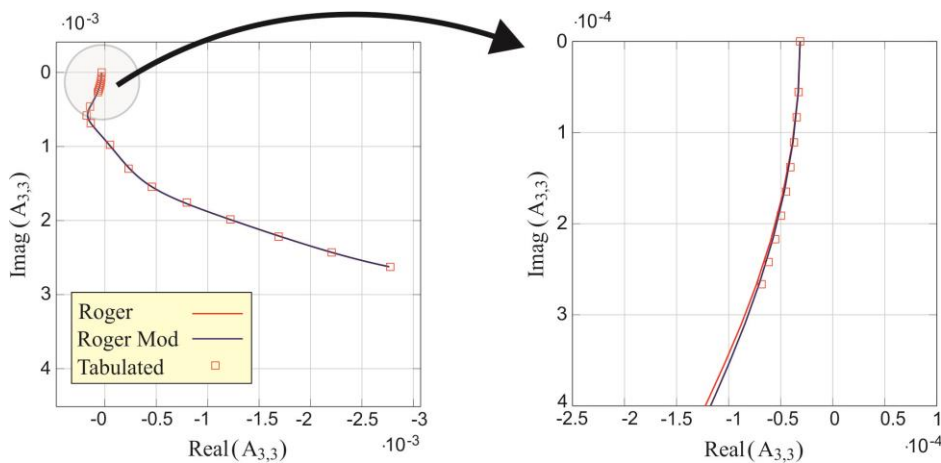


Figure 8: Comparison of different RFA methods on a set of 21 values of reduced frequencies on the element $A_{3,3}$ (proportional to $C_{M\alpha}$). Magnification of the area relative to small reduced frequencies is provided ($k \rightarrow 0$).

While Fig. 8 shows a good interpolation of the tabulated data for the element $A_{3,3}$ in the region of $k \rightarrow 0$ for both the chosen RFA methods, Fig. 7 shows how using Roger Mod, and thus adding a constraint on the first derivative of the interpolating function at small reduced frequencies, enhances the quality of the interpolation of the tabulated data for the element $A_{2,3}$. This results in a better prediction of the short period for UFFD using Roger Mod in Fig. 6(b) (better matching with RFD results) if compared to the UFFD using Roger method shown in Fig. 6(a). It is worth to underline that even if Roger Mod embeds a further constraint on the first derivative of the interpolating function for the aerodynamic forces at $k = 0$, the Least-square methods, which the RFA is based on, minimizes the error on the whole set of equations, not ensuring the correct value of the derivative but globally increasing the accuracy of the interpolation in the low reduced frequency area.

It is clear, from the presented results, that the choice of the RFA method deeply influences the output of the UFFD analyses. It seems that the quality of the RFA in the $k \rightarrow 0$ region plays a crucial role in the prediction of the flight-dynamic characteristics of a rigid configuration.

Now, the same set of analyses is performed interpolating the aerodynamic forces over the first 6 values of the original set of reduced frequencies: the new set covers a considerably smaller interval of reduced frequencies around $k = 0$. Again, Fig. 9 shows the root loci for the RFD and UFFD of the rigid vehicle for two chosen RFA methods, Fig. 10 the interpolation over the set of the chosen reduced frequencies, provided by the different RFA methods for elements $A_{2,3}$ and $A_{3,3}$.

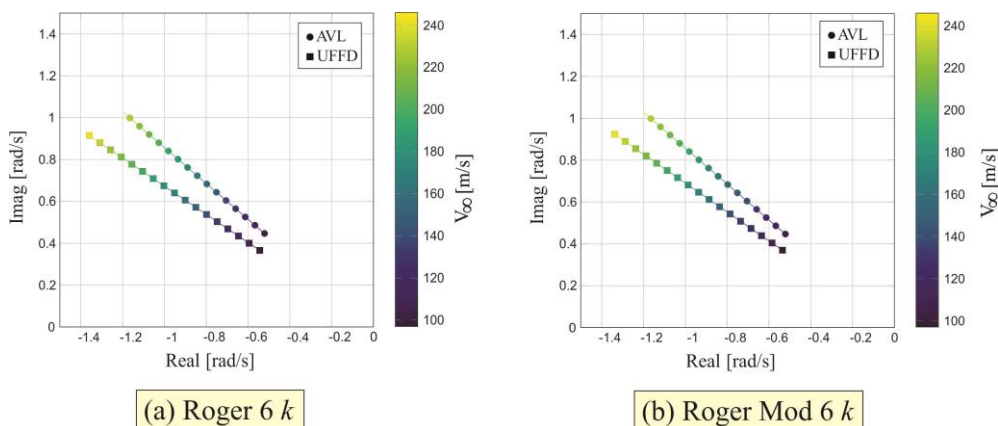


Figure 9: PrP250 MTOW, rigid flight-dynamics: comparison between RFD (AVL based aerodynamic model) and UFFD for rigid-body (DLM based aerodynamic model). 6 values of k , sea level.

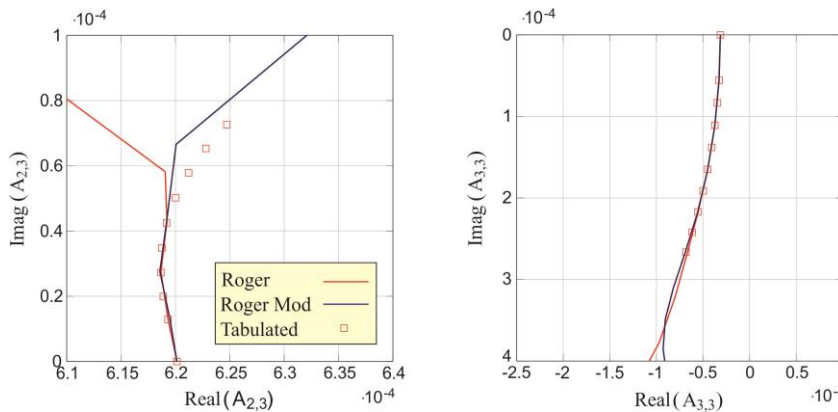


Figure 10: Comparison of different RFA methods on a set of 21 values of reduced frequencies and on the element $A_{2,3}$ (proportional to $C_{L\alpha}$) on the left and the element $A_{3,3}$ (proportional to $C_{M\alpha}$) on the right.

Being considerably lower the number of reduced frequencies, these RFAs both perform very well in the given domain, as shown in Fig. 10. As a result, UFFD eigenvalues are quite similar in Fig. 9(a) and Fig. 9(b). Additionally, the behaviour of interpolating functions beyond the first 6 reduced frequencies is absolutely poor. It is consequently possible to state that the flight dynamics of a rigid vehicle is marginally affected by values of unsteady aerodynamic forces relative to reduced frequencies far from the region of $k = 0$.

A question may arise spontaneously, then: why, if the interpolation method is good, still, such a difference exists between the values of the RFD and rigid UFFD? The answer relies in the different aerodynamic models employed: AVL is based on a steady VLM which can only calculate steady aerodynamic derivatives. The DLM, on the contrary, is an unsteady method and evaluates aerodynamic forces that are proportional to unsteady aerodynamic derivatives, such as $C_{M\dot{\alpha}}$ and $C_{L\dot{\alpha}}$ [18]. Fig. 11 shows how, increasing the module of $C_{M\dot{\alpha}}$ (negative in sign), RFD's short period reduces its imaginary part at every considered speed, recovering the values evaluated by UFFD.

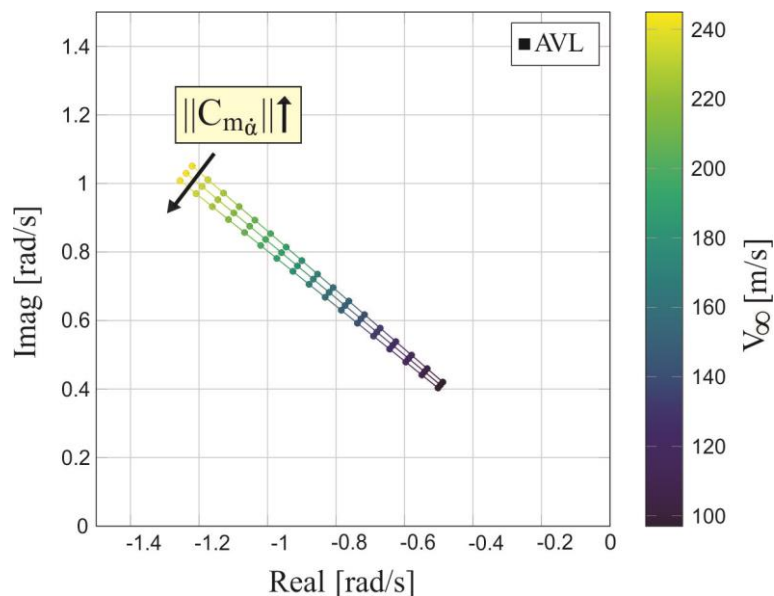


Figure 11: Influence of the derivative $C_{M\dot{\alpha}}$ on the short-period pole evaluated by RFD. The impossibility of AVL to calculate it justifies the discrepancies between the two approaches in the evaluation of the short period.

Another way to face the problem is trying to recover RFD results starting from the UFFD's short period and eliminating unsteady contributes from the GAF matrix. [Baldelli] shows how it is possible to give a physical interpretation to most of the entries of the matrices $[A_0]$, $[A_1]$ and $[A_2]$ of Eq. 3 *in case of a quasi-steady formulation of the aerodynamic forces*: contributions proportional to unsteady aerodynamic matrices given by the DLM can be, so, selectively eliminated. Fig. 12 illustrates this concept. Given UFFD's short period for a quasi-steady representation of the aerodynamic forces, it is shown how eliminating all the contributions proportional to $C_{M\dot{\alpha}}$ in the aerodynamic force matrices is enough to get a close representation of RFD's short period. The other unsteady contributions (such as the ones proportional to $C_{L\dot{\alpha}}$) play a very little role in describing the unsteady response.

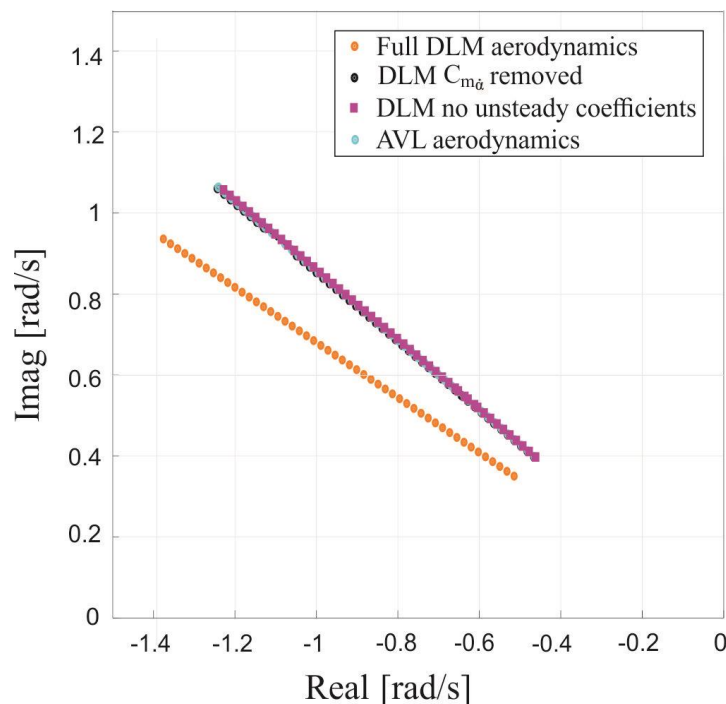


Figure 12: Influence of the unsteady aerodynamics in characterizing the short-period response given by UFFD. The most important effects are the contributions proportional to the derivative $C_{M\dot{\alpha}}$.

One issue remains open: even if it can be stated that results provided by the current tool UFFD are more accurate as featuring unsteady aerodynamic effects, it is not yet possible to judge the goodness of the estimation of $C_{M\dot{\alpha}}$ as evaluated by the DLM without recurring to more sophisticated aerodynamic calculations based on CFD or to tunnel tests (also given the non-conventional wing layout under exam).

5 MTOW CONFIGURATION: LONGITUDINAL ELASTIC UFFD ANALYSIS

After analysing flight-mechanics characteristics of the rigid vehicle, unified analyses are performed through UFFD with the purpose of identifying effects of mutual interaction between the rigid flight dynamics and the aeroelastic behaviour of the configuration. The elastic modes of the free-flying configuration have already been shown in Fig. 4.

As a mean of comparison, following the same strategy already used in [14,15]. The unified analysis of the free-flying configuration is compared with flutter results of the *cantilever* wing-system showed in Fig. 2. The comparison is able to highlight the different behaviours induced by the presence of rigid

modes on the flutter response. Differently than the previous studies, anyway, this time the fully unified model takes into account the vehicle's flight-dynamics, the rigid mode properly assumes the meaning of short period and it is possible to compare its response to the case of rigid aircraft, already discussed.

For both the configurations, aerodynamic forces are evaluated through the DLM over a set of 21 reduced frequencies, representative of the number of elastic modes proved to give convergence of results in flutter analyses for the given free-flying structural model (first 25 elastic modes). Forces are evaluated without compressibility correction at Mach = 0. Roger Mod is the chosen RFA method. Figure 13 shows the real and imaginary part of the eigenvalues for the considered range of speeds.

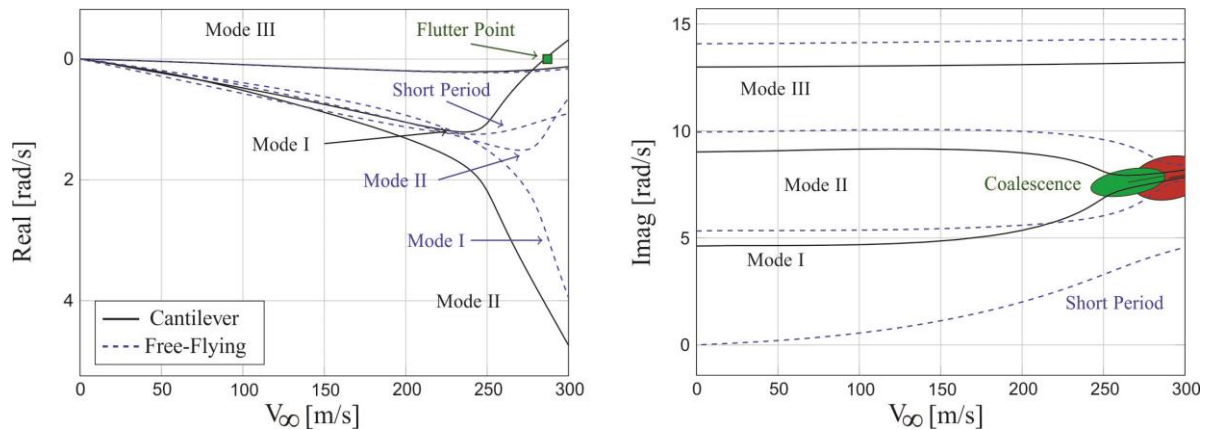


Figure 13: PrP250 MTOW. Real and imaginary parts of the eigenvalue of the system at different speeds: comparison between cantilever and UFFD response; sea level.

As seen from Figure 13 for the cantilever configuration flutter occurs at 287 m/s while the free-flying configuration is flutter-free in the considered speed range, up to 300 m/s. This confirms the trend already seen in [14] where, in the interpretation given to the phenomenon, considering the fuselage inertial properties of the MTOW configuration, the rigid mode (short-period mode) interacts with the first elastic mode, postponing the coalescence of the first two elastic modes responsible of flutter insurgence.

5.1 Flight quality analysis: comparison between rigid and elastic configuration

This section is focused on the flight-dynamic properties of the flexible vehicle and, in particular, on the analysis of the short-period mode. The comparison of the short period for flexible and rigid vehicle at sea-level and with the same RFA method is presented in Fig. 14.

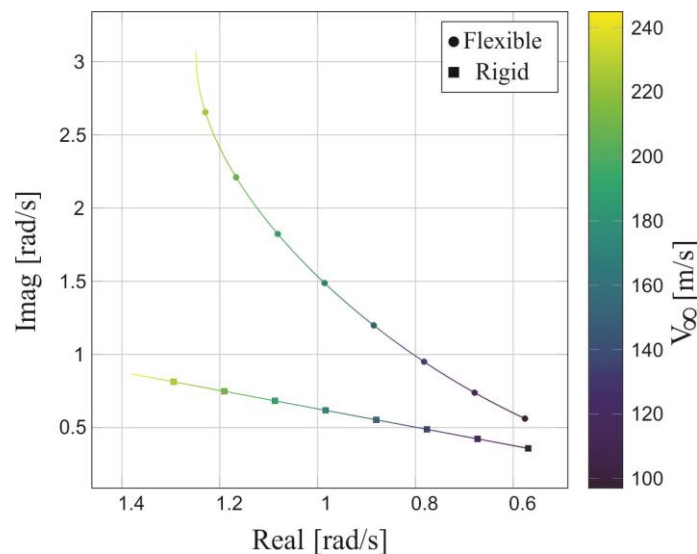


Figure 14: PrP250 MTOW. comparison of short-period mode for rigid-body and flexible vehicle; Roger Mod RFA, sea level.

The two branches have the same origin but as speed increases, progressively deviate from each other: the flexible branch moves upward and then bends towards the imaginary axis for higher speeds. As already discussed this behavior is due to the interaction with Mode I (elastic) with the same mechanism that postpone flutter point in the free-flying configuration.

At this point some considerations concerning the vehicle's flight qualities can be made for both the rigid and the unified model. The flying qualities of an aircraft are strictly related to physical flight parameters, both static, such as the margin of stability, and dynamic, like natural frequencies and damping ratio of rigid-body modes. MIL-F-8785C [32] provides requisites to characterize a vehicle's flying qualities. Such requisites involve the open loop system's response to the pilot control and are expressed as constraints on the poles representing the flight dynamics of the vehicle. In longitudinal dynamics constraints are provided for both long period and short-period poles, both under the point of view of damping ratio and frequency. Here some considerations will be made about the short-period damping ratio only. The given requirements are based on three different levels of flying qualities (1 is the best, 3 is sufficient). The aircraft class and the chosen flight phase (given by the category) determine the specific values to be fulfilled given the aircraft, as shown in Table 3.

Table 3: Flying Quality Level requirement for short-period damping ratio; aircraft of class III

Requirements		
Categories A and C	Category B	Flying Quality Level
$\zeta_{SP} > 0.35$	$\zeta_{SP} > 0.30$	1
$\zeta_{SP} > 0.25$	$\zeta_{SP} > 0.20$	2
$\zeta_{SP} > 0.15$	$\zeta_{SP} > 0.15$	3

Table 4 resumes the study of the short period conducted with the UFFD tool for both rigid and flexible cases, at sea level (Figure 14) and cruise level ($h=10500m$) for the given speeds. For the sake of clarity, only parameters for cruise speed at both considered altitudes are given. Comparing the data in Table 4 with the requirements in Table 3 it is showed how the considered configuration fully fulfills the requirements on short-period damping ratio both for the rigid case than for the flexible one, for all categories. Worth to underline is the significant reduction of ζ_{SP} from rigid vehicle to flexible one (41% at sea level and 35% at cruise, for the given speeds) that reveals how the flexibility of the aircraft is a fundamental parameter to take in consideration for the study of its flying qualities.

Table 4: PrP250 MTOW: short-period dynamic properties at sea level ($h = 0 m$ and $V = 196 m/s$) and cruise ($h = 10500 m$ and $V = 252 m/s$).

	Sea level		Cruise	
	Rigid	Flexible	Rigid	Flexible
Eigenvalue	$-1.12 + i0.70$	$-1.11 + i1.94$	$-0.44 + i0.59$	$-0.44 + i1.03$
$\omega_{n,SP} [s^{-1}]$	1.32	2.24	0.74	1.13
ζ_{SP}	0.85	0.50	0.60	0.39

6 QZFW CONFIGURATION: LONGITUDINAL RIGID FLIGHT-DYNAMIC AND ELASTIC UFFD ANALYSIS

Initial steps are here made towards the characterization of different load conditions. The QZFW configuration is studied both with a rigid flight dynamics and an elastic UFFD approach, same as already seen in Sections 5 and 6. Table 5 contains the aerodynamic derivatives of the configuration according to AVL. The reduced values of $C_{M\alpha}$ highlights the new margin of stability. Small influences are seen (as explained) also in the values of C_{Lq} and C_{Mq} . For the root loci, the considered speed range is the same as for the case of MTOW since they cover part of the flight envelope.

Table 5: PrP250 QZFW: AVL rigid-body longitudinal stability derivatives

$C_{L\alpha}$	4.43 1/rad
$C_{M\alpha}$	- 0.13 1/rad
C_{Lq}	5.43
C_{Mq}	-28.73

6.1 Longitudinal rigid flight-dynamics

The rigid flight-dynamics of the QZFW configuration is studied in this section; again, as a mean of comparison, both a classical RFD model (VLM-AVL based aerodynamic model) and UFFD for rigid-body (DLM based aerodynamic model) have been employed.

Again, it is found that an adequate use of the RFA, capable of best fitting the DLM aero forces at small reduced frequencies, is essential to achieve good results, as already explained in Sec. 4: in this case Roger Mod over the first 6 of the original set of 21 reduced frequency has been found as the best compromise. The comparison between RFD and UFFD is presented in Fig. 15.

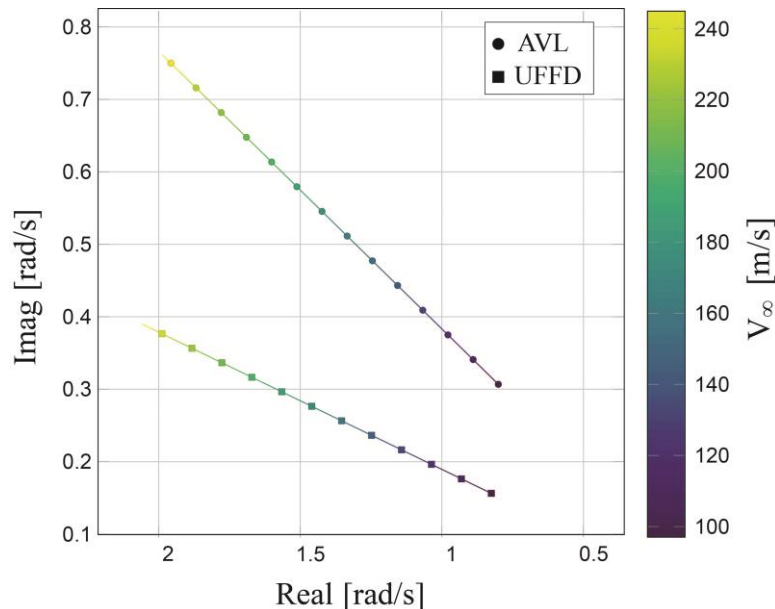


Figure 15: PrP250 QZFW, rigid flight-dynamics: comparison between RFD (AVL based aerodynamic model) and UFFD for rigid-body (DLM based aerodynamic model). Roger Mod RFA over 6 k , sea level.

In this case, particularly influent is the contribution given by unsteady aerodynamic forces for the UFFD case, if compared to RFD. Same observations can be made as already done concerning Fig. 11 and Fig. 12.

6.2 Elastic UFFD analysis

Unified analysis is performed at sea level and compared to the MTOW case. Fig. 16 groups the results in form of real and imaginary parts of eigenvalues for both the QZFW and the MTOW configuration. Concerning the QZFW configuration, it is possible to notice how the coalescence of the first two elastic modes is now fully postponed beyond the considered speed range. However, the configuration is not flutter free as the third mode becomes unstable at a speed of $V = 285 \text{ m/s}$. It is opinion of the authors that this new scenario is due to the fundamental new modal behaviour of the fuel-free configuration, as already stated commenting Fig. 4.

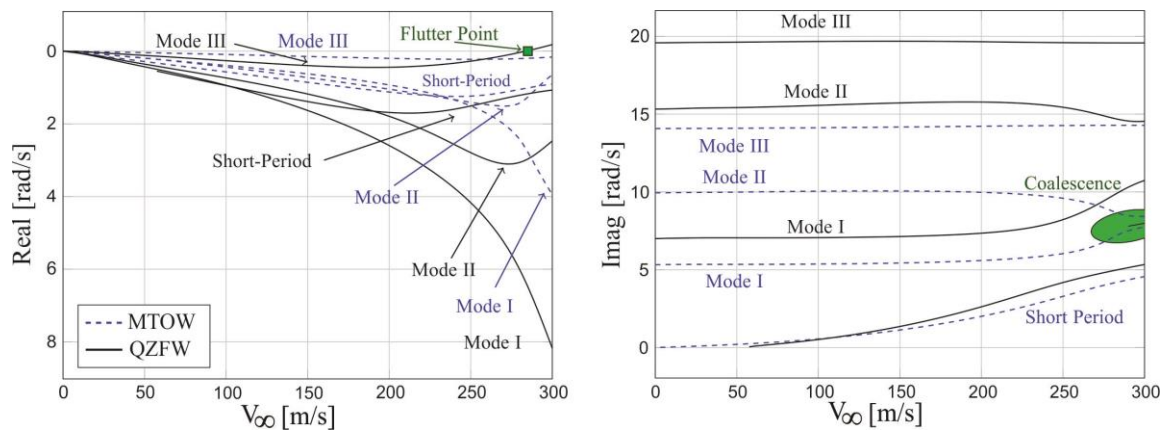


Figure 16: PrP250 QZFW vs MTOW, root locus for the UFFD analysis. Real and imaginary parts of the eigenvalue of the system at different speeds; sea level.

6.3 Flight quality analysis: comparison between rigid and elastic configuration

The comparison of the short period for flexible and rigid vehicle at sea-level and with the same RFA method is presented in Figure 14. The scenario is similar to the MTOW case but, here, the influence of the elasticity is stronger than in the MTOW case *at higher speeds*: a stronger interaction with the first elastic mode than in the MTOW case can be noticed in Fig. 17.

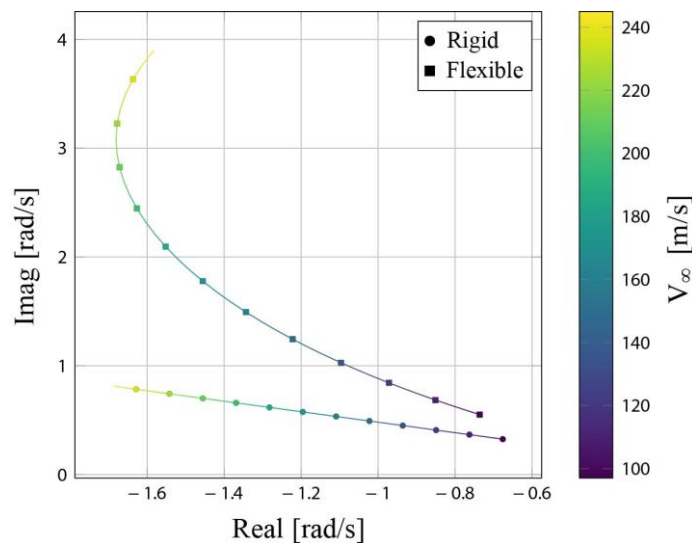


Figure 17: PrP250 QZFW, comparison of short-period mode for rigid-body and flexible vehicle; Roger Mod RFA over 21 k; sea level.

For the cruise speeds, at both altitudes, short-period dynamic properties are given in Table 6. Situation is similar to what we found in the MTOW case: regulation is fulfilled for every category but, still, a sensitive reduction of the damping ratio due to elasticity of the vehicle can be noticed: 39% at sea level and 44% at cruise.

Table 6: PrP250 QZFW: short-period dynamic properties at sea level ($h = 0 \text{ m}$ and $V = 196 \text{ m/s}$) and cruise ($h = 10500 \text{ m}$ and $V = 252 \text{ m/s}$).

	Sea level		Cruise	
	Rigid	Flexible	Rigid	Flexible
Eigenvalue	$-1.36 + i0.66$	$-1.61 + i2.44$	$-0.7 + i0.42$	$-0.69 + i1.25$
$\omega_{n,SP} [s^{-1}]$	1.52	2.93	0.82	1.43
ζ_{SP}	0.9	0.55	0.86	0.48



7 CONCLUSIONS

This work has contributed to shed light over the longitudinal flight-dynamic behaviour of a *flexible* PrandtlPlane. An in-house unified state-space tool has been written, which solves the equation of motion of an elastic aerodynamic body and evaluates its flight-dynamic and aeroelastic stability. Such tool embeds a Doublet Lattice Method for the evaluation of unsteady aerodynamic forces.

First, rigid analyses are performed over the Maximum Payload Maximum Take-Off Weight with maximum payload load case of the configuration, to evaluate longitudinal stability. A good interpolation of the aerodynamic force matrix at small reduced frequencies plays a critical role. Moreover, the ability of predicting unsteady aerodynamic forces adds further value to the method when compared to tools embedding only steady aerodynamics, since aerodynamic derivatives as $C_{M\dot{\alpha}}$, contributing to the stability properties, can be evaluated. The Short-period pole is found stable over the considered range speed and its damping ratio satisfying the Flying Quality Level Requirements.

Second, the elastic configuration is analysed with the purpose of identifying mutual interaction between the rigid flight-mechanic and aeroelastic behaviour of the configuration. Given the presence of the short-period mode, flutter speed increases if compared to the cantilever wing-system configuration. The rigid mode, in fact, interacts with the first elastic mode, postponing the flutter point (due to the coalescence of the first two elastic modes' branch) beyond the considered speed range. The short period itself is considerably influenced by the vehicle's elasticity: the damping ratio experiences a reduction up to the 41% at sea level for cruise speed.

Last contribution is the study of a different load case of the same configuration carrying a residual amount of fuel and having a reduced margin of stability. Rigid flight mechanics shows the same range of poles relative to short period as for the MTOW configuration. Here, anyway, results have been noticed to be more sensitive to the chosen RFA. Moreover, unsteady aerodynamic contributions, as calculated by the DLM, have more influence in shifting results from the ones of tools based on steady aerodynamics. The study of the elastic configuration reveals an instability of the third elastic mode which results in a flutter point of $V = 285 \text{ m/s}$. The new instability is justified by the different modal properties of the load case: the different weight-to-stiffness ratio of the wing without fuel modifies the higher-frequency elastic modes in terms of shape and associated frequency. Again, the short-period response is influenced by the elasticity, especially at higher speeds; anyway, values of the damping ratios at cruise speeds for both the analysed altitudes comply with regulations.

REFERENCES

1. E. Albano, W. P. Rodden; 1969; "A doublet-lattice method for calculating lift distributions on oscillating surfaces in subsonic flows."; *AIAA Journal*; **7**(2); pp. 279-285.
2. W. P. Rodden, P. F. Taylor, S. C. McIntosh; 1998; "Further Refinement of the Subsonic Doublet-Lattice Method", *Journal of Aircraft*; **35**(5); pp. 720-727.
3. K. L. Roger; 1977; "Airplane math modelling methods for active control design."; AGARD-CP-228; pp.4-1.
4. M. Karpel; 1982; "Design for Active Flutter Suppression and Gust Alleviation Using State-Space Aeroelastic Modeling"; *Journal of Aircraft*; **19**(3); pp. 221-227.
5. M. Karpel; 1981; "Design for active and passive flutter suppression and gust alleviation."; *PhD Thesis*; Stanford University; Stanford (CA).
6. D. Dal Canto, A. Frediani, G. L. Ghiringhelli, M. Terraneo; 2012; "The Lifting System of a PrandtlPlane, Part 1: Design and Analysis of a Light Alloy Structural Solution"; G. Buttazzo, A. Frediani; *Variational Analysis and Aerospace Engineering: Mathematical Challenges for Aerospace Design*; **66**; Springer US; pp. 211-234.
7. E. Rizzo; 2009; *Optimization Methods Applied to the preliminary designed of innovative non conventional aircraft configurations*, Edizioni ETS.
8. E. Rizzo, A. Frediani; 2009; "Application of Optimization Algorithms to Aircraft Aerodynamics"; G. Buttazzo, A. Frediani; *Variational Analysis and Aerospace Engineering: Mathematical Challenges for Aerospace Design*; **33**; Springer US; pp. 419-446.



9. D. Dal Canto; 2009; "Progetto preliminare del cassone alare di un velivolo Prandtl-Plane mediante l'applicazione di un metodo di ottimizzazione strutturale "; *Master Thesis*; Dipartimento di ingegneria Aerospaziale, Università di Pisa; Pisa.
10. M. Voskuijl, J. de Klerk, D. van Ginneken; 2012; "Flight Mechanics Modeling of the PrandtlPlane for Conceptual and Preliminary Design"; G. Buttazzo, A. Frediani; *Variational Analysis and Aerospace Engineering: Mathematical Challenges for Aerospace Design*; **66**; Springer US; pp. 435-462.
11. D. van Ginneken, M. Voskuijl, M. van Tooren, A. Frediani; 2010; "Automated Control Surface Design and Sizing for the Prandtl Plane"; *51st AIAA/ASME/ASCE/AHS/ASC Structures, Structural Dynamics, and Materials Conference*; **AIAA 2010-3060**; Orlando, Florida; 12-15 April 2010.
12. N. Divoux, A. Frediani; 2012; "The Lifting System of a PrandtlPlane, Part 1: Design and Analysis of a Light Alloy Structural Solution"; G. Buttazzo, A. Frediani; *Variational Analysis and Aerospace Engineering: Mathematical Challenges for Aerospace Design*; **66**; Springer US; pp 211-234.
13. C. Dimartino, M. Baldini; 2009; "Analisi agli elementi finite di un tronco di fusoliera di un velivolo PrandtlPlane sottoposto a carichi limite di pressurizzazione e di massa"; *Master thesis*; Università di Pisa, Pisa.
14. R. Cavallaro, R. Bombardieri, L. Demasi; A. Iannelli; 2015; "PrandtlPlane Joined Wing: Body Freedom Flutter, Limit Cycle Oscillation and Freeplay Studies"; *Journal of Fluid and Structures*; **59**; pp. 57-84.
15. R. Bombardieri, R. Cavallaro, L. Demasi; "A Historical Perspective on the Aeroelasticity of Box Wings and PrandtlPlane with New Findings"; *57th AIAA/ASCE/AHS/ASC Structures, Structural Dynamics, and Materials Conference, 3rd AIAA SciTech*; **AIAA 2016-0238**; San Diego, California; 4-8 January 2016.
16. F. Oliviero, D. Zanetti, V. Cipolla; 2015 "Flight dynamics model for preliminary design of PrandtlPlane wing configuration with sizing of the control surfaces"; *Aerotecnica Missili & Spazio*; **95(4)**; pp. 201-210.
17. M. Drela, H. Youngren; 2017; "AVL, Aerodynamic Analysis, Trim calculations, Dynamic Stability Analysis, Air Configuration Development"; <http://web.mit.edu/drela/Public/web/avl/>;
18. D. H. Balelli, P. C. Chen, J. Panza; 2006; "Unified aeroelastic and flight dynamic formulation via rational function approximations"; *Journal of Aircraft*; **43(3)**; pp.763-772.
19. J. de Klerk; 2010; "Design and integration of a propulsion system for the PrandtlPlane"; *Master Thesis*; T. U. Delft; Delft, Netherlands.
20. F. Auricchio; 2016; "Development of a Framework for Unified Flight-Dynamic and Aeroelastic Analysis"; *Master thesis; Università Federico II di Napoli; Napoli*.
21. R. D. Milne; 1962; *Dynamics of the Deformable Airplane*; Her Majesty's Stationary Office; **3345**.
22. R. D. Milne; 1968; "Some Remarks on the Dynamics of the Deformable Airplane"; *AIAA Journal*; **6(556)**.
23. B. Etkin; 1972; J. Wiley and Sons; *Dynamics of atmospheric flight*; New York
24. M. R. Waszak, D. K. Schmidt; 1988; "Flight Dynamics of Aeroelastic Vehicles"; *Journal of Aircraft*; **25(6)**; pp. 563-571.
25. L. Meirovitch, H. D. Nelson; 1966; "On the high-spin motion of a satellite containing elastic parts."; *Journal of Spacecraft and Rockets*; **3(11)**; pp. 1597-1602.
26. L. Meirovitch; 1991; "Hybrid state equations of motion for flexible bodies in terms of quasi-coordinates"; *Journal of Guidance, Control, and Dynamics*; **14(5)**; pp. 1008-1013.
27. R. Cavallaro and L. Demasi, "Challenges, Ideas, and Innovations of Joined-Wing Configurations: A Concept from the Past, an Opportunity for the Future," *Progress in Aerospace Sciences*, vol. 87, pp. 1-93, 2016.
28. G. H. N. Looye; 2008; "An Integrated Approach to Aircraft Modelling and Flight Control Law Design"; *PhD Thesis; T. U. Delft; Delft*.
29. A. Frediani; 2002; "New Large Aircraft"; EP 071697B1.
30. A. Frediani; 2003; "Velivolo biplane ad ali contrapposte"; Italy; FI 2003A000043.
31. D. K. Schmidt; 2012; *Modern Flight Dynamics*; McGraw-Hill.
32. MIL-F-8785C; 1980; "flying qualities of piloted airplanes"; *Technical report, USA Military Specification*; http://www.mechanics.iei.liu.se/edu_ug/tmme50/8785c.pdf;